Multiple Coulomb phases with temperature-tunable ice rules in pyrochlore spin-crossover materials

Jace Cruddas [*] and B. J. Powell [†]
School of Mathematics and Physics, The University of Queensland, QLD 4072, Australia

(Received 29 July 2020; revised 17 June 2021; accepted 9 July 2021; published 27 July 2021)

Spin-crossover (SCO) molecules have two accessible states: one high spin (HS) and one low spin (LS). We show that on the pyrochlore lattice elastic interactions between SCO molecules can give rise to three different spin-state ice phases (denoted H_nL_{4-n} with $n = 1$, 2, or 3)—characterized by the "ice rules" that every tetrahedron must contain n HS and $4 - n$ LS metals. Each is a "Coulomb phase" where a local ice rule can be mapped to a divergence-free gauge field and the low-energy excitations carry a spin fractionalized midway between the LS and HS states. To date, no phase with the $n = 1$ and $n = 3$ ice rules has been observed. In SCO materials, the subtle competition between the entropies and enthalpies of the HS and LS states allows temperature or pressure to change the ice rules, allowing straightforward access to the $n = 1$ and $n = 3$ phases.

DOI: 10.1103/PhysRevB.104.024433

I. INTRODUCTION

In spin ices, such as $Dy_2Ti_2O_7$ and $Ho_2Ti_2O_7$, the magnetic Dy (Ho) atoms form a pyrochlore lattice composed of vertex sharing tetrahedra [1,2]. The combination of the crystal field [3,4] and the long-range dipolar interaction [5,6] constrain the magnetic moments to obey the two-in/two-out ice rule: Two of the spins point in to each tetrahedron and two point out. The number of ways of satisfying the ice rule grows with the size of the system, leading to an extensive zero-point entropy [4,7]. The ice rule can be mapped onto a divergence-free flux, analogous to constraints in magnetostatics and electrostatics. Violations of the ice rule carry a fraction of the magnetic spin degree of freedom, behaving effectively as magnetic monopoles with an emergent Coulombic interaction between them [8–10]. Spin ices are therefore said to be in a "Coulomb phase," which could also arise in frustrated antiferromagnets and some quantum spin liquids [11–14].

Coulomb phases can also arise from other degrees of freedom. Three coexisting Coulomb phases, each obeying two-in/two-out (or, more strictly, divergence-free) ice rules, are observed in the charge, atom displacement, and spin configurations of $CsNiCrF_6$ [15].

It was proposed, in the 1950's, that ices obeying the 1:3 or 3:1 ice rules should also occur [16]. However, to date, such phases have yet to be observed, although an ordered phase containing 1:3 and 3:1 tetrahedra has been reported [17]. For the nearest-neighbor Ising model on the pyrochlore lattice with collinear spins S_i, then, up to a constant,

$$\mathcal{H}_I = J\sum_{\langle i,j\rangle} S_iS_j + B\sum_i S_i = J\sum_\alpha (L_\alpha + B/4J)^2, \qquad (1)$$

where $L_\alpha = \sum_{i\in\alpha} S_i$ and α labels the tetrahedra. The ground state is clearly achieved whenever the magnitude of the "flux," $L_\alpha + B/4J$, is minimized for all α. Ice rules require the same value of L_α on all tetrahedra. Therefore, sweeping the field B moves the ground state between different ice rules. However, in spin ices the spins are not collinear and so one cannot simply apply a magnetic field to change the ice rules in these systems.

Recently, it has been proposed that spin-state ice (SSI) phases can occur in spin-crossover materials on the kagome lattice [18]. SSIs naturally contain two simultaneous ices as changes in the spin state and the structure of the coordination sphere change mutually. Here, we show that three different SSI phases arise for spin-crossover materials on the pyrochlore lattice: With the ice rules that each tetrahedron must contain n high-spin (HS) and $(4 - n)$ low-spin (LS) metal centers, the three phases we find correspond to $n = 1$, $n = 2$, and $n = 3$. Furthermore, we show that sweeping either temperature or pressure alone is sufficient to tune between SSI phases obeying three different ice rules. This is a direct consequence of the competition between the single-molecule spin-crossover behavior and the elastic interactions between molecules in a crystal. We predict that pinch point singularities, the *sine qua non* of the Coulomb phase, will be detectable via neutron scattering in small magnetic fields and that the low-energy excitations are deconfined and carry a spin midway between that of the two spin states of a single molecule.

Spin crossover (SCO) occurs in transition metal complexes and frameworks when the low-spin (LS, e.g., $t_{2g}^6e_g^0$, $S = 0$) and high-spin (HS, e.g., $t_{2g}^4e_g^2$, $S = 2$) states have comparable enthalpy. SCO provides a reversible molecular switch, which is addressable by changes in temperature, pressure, light irradiation, magnetic field, and chemical environment [19]. As spin-state changes are accompanied by changes in molecular volume, color, and magnetic susceptibility, SCO materials are intrinsically multifunctional and have been widely explored for applications such as high-density reversible memory, and ultrafast nanoscale switches [19–21]. However, many questions about the fundamental physics at play in these systems remain open [22–36].

[*] j.cruddas@uq.edu.au
[†] powell@physics.uq.edu.au

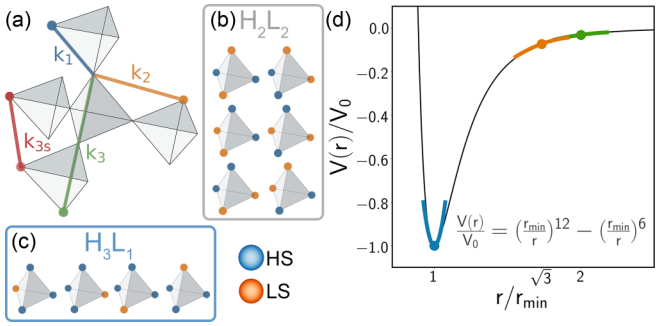

FIG. 1. (a) Pyrochlore lattice with the three nearest-neighbor interactions (k_1, k_2, and k_3) marked. We neglect through-space interactions between third nearest neighbors k_{3s} as we expect these to be much weaker than k_3. Ice rules in the (b) H_2L_2 and (c) H_1L_3 phases (H_3L_1 is equivalent to H_1L_3 upon reversing the colors). (d) For any reasonable potential between neighboring metals, near the minimum $\partial^2 V(r)/\partial r^2 \simeq k_1$ is positive and large (blue lines). At larger distances the second derivative is negative and decreases in magnitude with increasing distances (orange and green lines). Therefore, one expects $k_1 > 0$ and $k_2 < k_3 < 0$.

The weak magnetic interactions in most SCO materials means that the fraction of HS molecules $n_{\rm HS} \sim \chi T$. Hence the magnetic susceptibility χ is commonly used as a diagnostic for the cooperative behavior in the system—χT displays a step at a (first-order) transition between the HS and LS phases. Strongly cooperative behaviors often give rise to multiple step transitions [19,36–40]. The intermediate plateaus often display long-range patterns of HS and LS metals, but several disordered phases have been reported [41–43].

II. MODEL AND METHODS

Changes in the molecular volume accompany spin-state switching due to the (de)population of antibonding e_g orbitals in the (LS) HS state: The metal-ligand bond length in the HS state is often ∼10% larger than that in the LS state. In molecular materials and frameworks, the local structural distortions caused by metals changing spin state couple to long-range elastic interactions [44]. It is convenient to introduce a pseudospin label for the spin state of each metal, $\sigma_i = 1$ (-1) if the ith molecule is HS (LS). Defining $R_{\rm HS}$ ($R_{\rm LS}$) to be the equilibrium distance between metals in the HS (LS) phases, we can write the equilibrium midpoint between neighboring metals as $\overline{R} + \delta(\sigma_i + \sigma_j)$, where $\overline{R} = (R_{\rm HS} + R_{\rm LS})/2$ and $\delta = (R_{\rm HS} - R_{\rm LS})/4$. The effective Hamiltonian of the system is

$$\mathcal{H} = \frac{\Delta G}{2}\sum_i \sigma_i + \sum_{n=1}^{3}\frac{k_n}{2}\sum_{\langle i,j\rangle_n}\{r_{ij} - \eta_n[\overline{R} + \delta(\sigma_i + \sigma_j)]\}^2, \tag{2}$$

where $\Delta G = \Delta H - T\Delta S$ is the free-energy difference between HS and LS metals, $\Delta H = H^{\rm HS} - H^{\rm LS}$ and $\Delta S = S^{\rm HS} - S^{\rm LS}$ are the enthalpy and entropy differences between the HS and LS states, respectively, k_n are the effective spring constants between nth nearest neighbors (see Fig. 1), the sum over $\langle i, j\rangle_n$ includes all nth nearest neighbors, r_{ij} is the instantaneous distance between sites i and j, and $\eta_n = 1, \sqrt{3}, 2, \ldots$ is the ratio of distances between the nth and first nearest-neighbor distances on the undistorted pyrochlore lattice.

The single-molecule contribution to the entropy ΔS arises from the change in the spin and orbital quantum numbers and vibrational frequencies between the HS and LS states [45]. The vibrational contribution is typically largest and endows a rather complicated temperature dependence on ΔS that depends on all of the vibrational frequencies in both electronic states. As we are not interested in any one complex and for simplicity, we set $\Delta S = 4k_B \ln 5$ below [46], a typical magnitude of Fe(II) complexes [47].

If a pairwise interaction between metal centers is expanded to an arbitrary order only terms of bilinear order in the pseudospin variables arise, because $\sigma_i^2 = 1$ [36]. However, there is no guarantee that any individual interaction will be minimized—only the total free energy is minimized—thus the k_n are not required to be positive. For physically and chemically reasonable potentials, if the nearest-neighbor distance is close to the minimum of the potential, then $k_1 > 0$, but k_2 and $k_3 < 0$ [36], as illustrated for the Lennard-Jones potential in Fig. 1(d).

Estimates of k_1 from measurements of the bulk modulus yield $k_1 \approx 10^4$–10^5 K/Å^2 [44], in good agreement with values calculated from first principles, e.g., $k \sim 8 \times 10^4$ K/Å^2 in $[{\rm Fe(pz)Pt(CN)_4}] \cdot 2\,{\rm H_2O}$ (pz=pyrazine) [22]. As $\delta \simeq 0.05$ Å [48] this means that $k_1\delta^2$ is of order $k_B T_{1/2}$, where $T_{1/2} = \Delta H/\Delta S$ is the temperature at which one expects $n_{\rm HS} = 1/2$, typically 100–400 K [36]. Thus the characteristic energy scales of the single-molecule physics ($k_B T_{1/2}$) and the interactions between molecules ($k_1\delta^2$) both play important roles in understanding SCO materials.

Inspired by recent progress in the synthesis of tetrahedral iron cages [49] we study model (2) on the pyrochlore lattice [Fig. 1(a)], where we expect $k_2 < k_3 < 0$ [Fig. 1(d)] and require $k_1 + 6k_2 + 4k_3 > 0$ for structural stability.

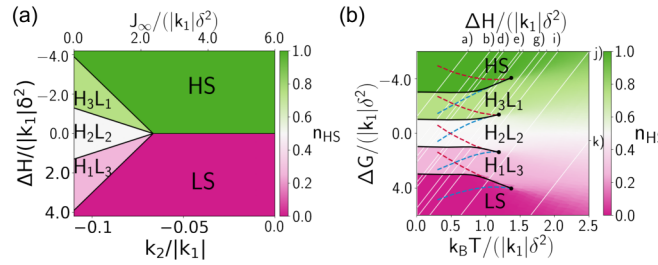

FIG. 2. (a) The zero-temperature phase diagram for $k_1 > 0$ and $k_3 = 3k_2/4$. For small $|k_2|$ the long-range strain dominates and picks out HS or LS states, but large $|k_2|$ suppresses this effect, allowing the SSI phases to emerge. (b) The finite-temperature phase diagram for $k_1 > 0$, $k_2 = -0.1k_1$, and $k_3 = -0.075k_1$. The colors of the phase diagram indicate the equilibrium values of the fraction of high spins $n_{\rm HS}$, calculated via parallel tempering. We find four (black) lines of first-order transitions that terminate at critical end points (black circles). The blue and red lines indicate lines of metastability (spinodals) for the cooling and heating calculations, respectively (cf. Fig. S1 [50]). Hence, the distance between blue and red lines is the width of the hysteresis. Individual materials have a fixed ΔH (white lines), and the corresponding HS fractions $n_{\rm HS}$ and heat capacities are shown in Figs. 4 and S2 [50], respectively.

We make the symmetric breathing mode approximation, which neglects asymmetric structural distortions [18,36], allowing the equilibrium distance to be written as $r_{i,j} = \eta_n x$, where x is the distance between nearest neighbors. We then minimize the resultant Hamiltonian over x, yielding a Ising-Husimi-Temperley model,

$$\mathcal{H} = \frac{\Delta G}{2}\sum_i \sigma_i + \sum_{n=1}^{3} J_n \sum_{\langle i,j\rangle_n} \sigma_i\sigma_j - \frac{J_\infty}{N}\sum_{i,j}\sigma_i\sigma_j, \qquad (3)$$

where $J_n = k_n\eta_n^2\delta^2$, the long-range strain $J_\infty = \sum_n z_n J_n$, and z_n is the coordination number for the nth nearest neighbor.

We calculate the finite-temperature properties from a combination of single spin-flip Monte Carlo, worm, and loop algorithms on a $12 \times 12 \times 12 \times 4 = 6912$ lattice except where stated [50]. We employ three different types of calculations: cooling, heating, and parallel tempering. The heating and cooling calculations simulate experiments under given conditions, giving the limits of metastability (spinodal lines), and hence the difference between the calculations corresponds to the width of the hysteresis. The parallel tempering calculations are designed to find the lowest free-energy state for a given set of parameters (including temperature).

III. RESULTS AND DISCUSSION

We find three distinct spin-state ice phases: H_3L_1, H_2L_2, and H_1L_3 (see Fig. 2). In the ground state of the H_nL_{4-n} phase every tetrahedron contains n HS and $4-n$ LS metals

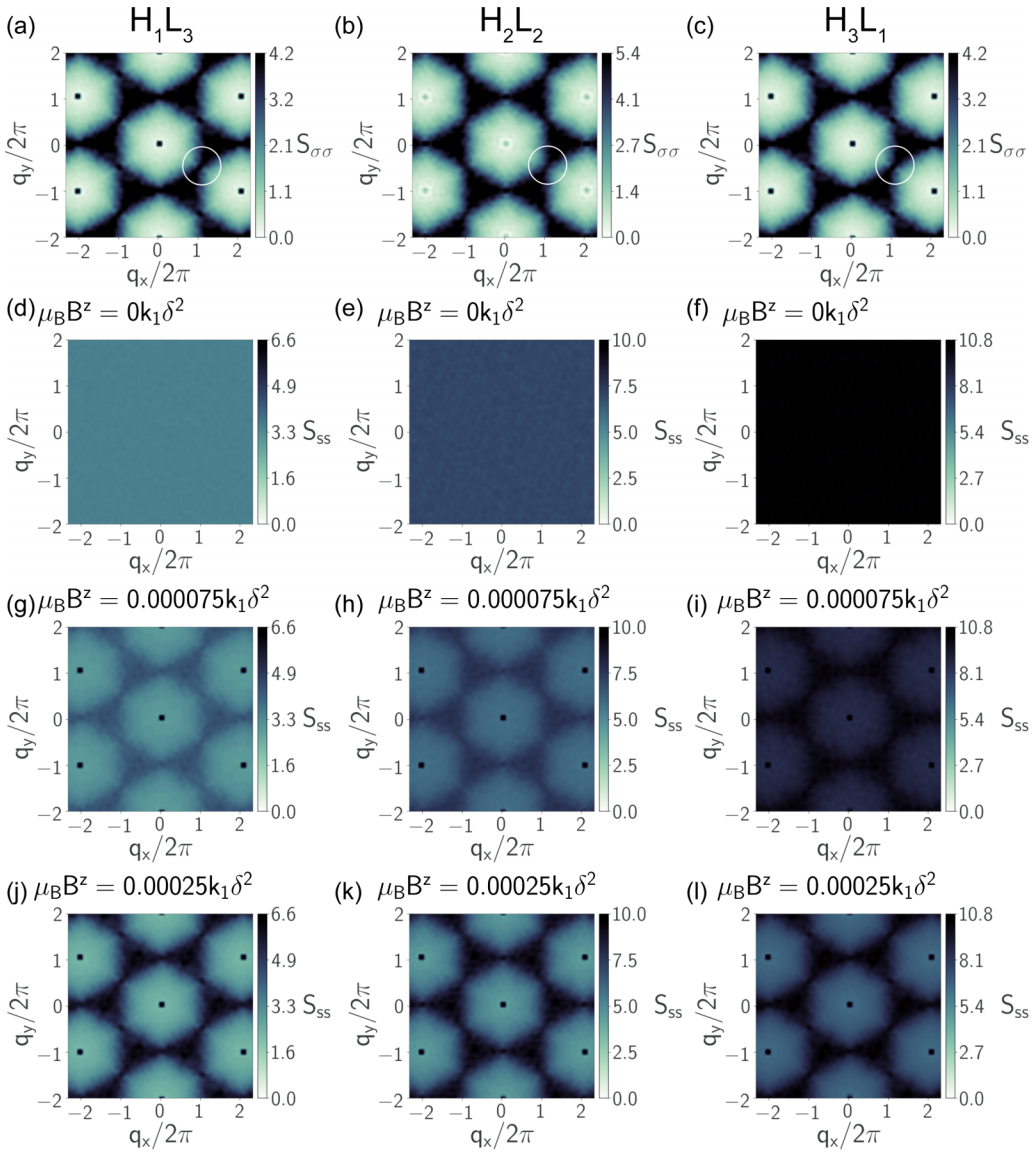

FIG. 3. (a)–(c) The structure factors $S_{\sigma\sigma}$ [Eq. (4)] for (a) H_1L_3, (b) H_2L_2, and (c) H_3L_1. All structure factors display pinch points, one of which is circled, at the Brillouin zone boundaries characteristic of a Coulomb phase [11]. (d)–(l) The spin structure factors S_{SS} [Eq. (5) for (d), (g), (j) H_1L_3, (e), (h), (k) H_2L_2, and (f), (i), (l) H_3L_1 at selected magnetic field strengths. For $k_1\delta^2 \sim 100$ K pinch points are observed for magnetic fields of <0.1 T, so only moderate fields are required for the pinch points to be observable via neutron scattering. All structure factors were calculated for $k_1 > 0$, $k_2/k_1 = 4k_3/3k_1 = -0.1$, and $k_BT/(k_1\delta^2) = 0.01$ on a $36 \times 36 \times 4 \times 4 = 20\,376$ lattice with (a), (d), (g), (j) $\Delta H = 2k_1\delta^2$, (b), (e), (h), (k) $\Delta H = 0$, and (c), (f), (i), (l) $\Delta H = -2k_1\delta^2$.

[Figs. 1(b) and 1(c)]. Thus, the H_3L_1 and H_1L_3 phases can be mapped onto the dimer model on a diamond lattice, and the H_2L_2 phase can be mapped onto the loop model on a diamond lattice [11]. We expect the stability of the ice phases to be *underestimated* in calculations because the long-range strain, which the favors ferroelastic (HS and LS) phases, goes to a constant at large separations in the symmetric breathing mode approximation [36], rather than decaying with a power law as expected physically [44].

In order to verify that the SSI phases at $T = 0$ are indeed Coulomb phases we have calculated the pseudospin structure factor [Figs. 3(a)–3(c)],

$$S_{\sigma\sigma}(\vec{q}) = \frac{1}{N^2}\sum_{ij}\langle\sigma_i\sigma_j\rangle e^{i\vec{q}\cdot\vec{r}_{ij}}. \tag{4}$$

We clearly observe singularities in $S_{\sigma\sigma}$ at the Brillouin zone boundary, known as pinch points, which are a direct consequence of the existence of a divergenceless gauge field [11]. This confirms that the intermediate plateaus are indeed Coulomb phases.

However, directly measuring the pseudospin structure factor is not straightforward. In SCO materials the magnetic correlations between sites are typically negligible. Therefore, the spins are described by a Zeeman Hamiltonian, $\mathcal{H}_Z = \sum_i \mu_B^z B S_i^z(\sigma_i)$, where the spin $\boldsymbol{S}_i(\sigma_i)$ depends on the spin state, B is the applied field, and μ_B is the Bohr magneton. The spin structure factor is

$$S_{\rm SS}(\vec{q}) \equiv \frac{1}{N^2}\sum_{ij}\langle \boldsymbol{S}_i(\sigma_i)\cdot\boldsymbol{S}_j(\sigma_j)\rangle e^{i\vec{q}\cdot\vec{r}_{ij}} \tag{5a}$$

$$= \left(\frac{m_+ - m_-}{2}\right)^2 S_{\sigma\sigma}(\vec{q}) + S_d(B^z), +S_B(B^z)\delta(q), \tag{5b}$$

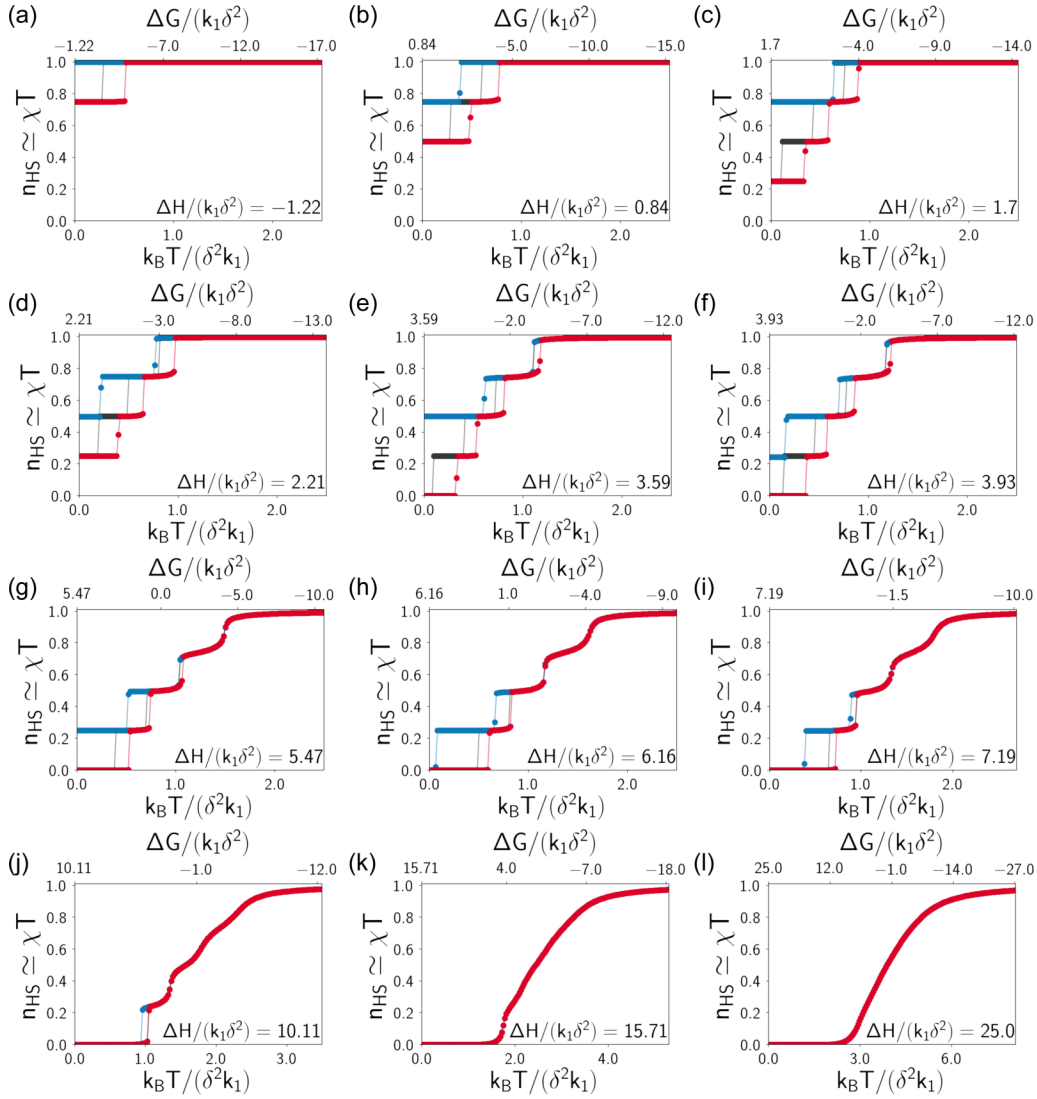

FIG. 4. The fraction of high spins $n_{\rm HS}$ for selected values of $\Delta H/(k_1\delta^2)$ with $k_1 > 0$ and $k_2/k_1 = 4k_3/3k_1 = -0.1$. The red, blue, and black lines represent heating, cooling, and parallel tempering calculations, respectively. The parallel tempering calculations return the state with the lowest free energy, while the heating and cooling calculations indicate the limits of metastability (spinodal lines). We find plateaus at $n_{\rm HS} \simeq 0$, $\frac{1}{4}$, $\frac{1}{2}$, $\frac{3}{4}$, and 1, corresponding to the LS, H_1L_3, H_2L_2, H_3L_1, and HS phases. Hence, for a wide range of parameters, it is possible to tune between different SSI phases with temperature alone. Snapshots of these phases are shown in Fig. S3 [50].

where $m_\pm = \sum_i \langle S_i^z(\pm 1)\rangle / N$, and the trivial diffuse, $S_d(B^z)$, and Bragg, $S_B(B^z)$, scattering are given by

$$S_d(B^z) = [S_H(S_H+1) - S_L(S_L+1) - m_+^2 + m_-^2]n_{\rm HS} + S_L(S_L+1) - m_-^2 \quad (6)$$

$$S_B(B^z) = \left(\frac{m_+ + m_-}{2}\right)^2 + \left(\frac{m_+^2 - m_-^2}{2}\right)(2n_{\rm HS} - 1). \quad (7)$$

This is directly measurable via neutron scattering and clearly shows the pinch points [Figs. 3(d)–3(l)]. Importantly, the fields required are modest. For a typical value of the intermolecular interactions $k_1\delta^2 \sim 100$ K, the magnetic fields required to observe pinch points are at < 0.1 T. Applied pressure favors the smaller LS state. Therefore, pressure would also allow one to tune between the three different SSI phases, and to do so at low T where the pinch points are most easily observed.

The ratio $\Delta H/(k_1\delta^2)$ not only has important consequences for the low-temperature physics, but also for the high-temperature behavior [Figs. 2(b) and 4]. For $\Delta H \sim -(k_1\delta^2)$ we observe a single first-order transition. This is a purely collective phenomenon, as every single ion always favors the HS state ($\Delta G < 0$ at any temperature). Increasing ΔH induces further transitions with plateaus at $n_{\rm HS} \simeq 0$, $\frac{1}{4}$, $\frac{1}{2}$, $\frac{3}{4}$, and 1, corresponding to the LS, H_1L_3, H_2L_2, H_3L_1, and HS phases, respectively [Figs. 4(b)–4(h)]. Hence, for a wide range of parameters, it is possible to tune between different SSI phases with temperature alone.

This can be understood as follows: The single-molecule entropy difference between spin states (ΔS) couples to the pseudospin just as a magnetic field couples to spin in the Ising model, Eq. (1). Thus, the single-molecule spin-crossover behavior acts as an effective temperature-dependent "field" for the pseudospins. This changes the ice rules as the temperature varies.

Due to the large width of the hysteresis loop at low temperatures, simulations of straightforward cooling do not always result in the same low-temperature phase as is found by parallel tempering [Figs. 4(a)–4(g). Similar effects have been observed experimentally in SCO materials that display long-range antiferroelastic order [51,52], and labeled "hidden hysteresis." The hidden low-temperature states can be realized by either photoswitching (i.e., reverse-light-induced excited spin-state trapping) or applying and adiabatically releasing a pressure to the system. Hence, it becomes possible to tune between different SSI phases with not only temperature but pressure and light as well. Thus, spin-crossover materials provide a rare opportunity to study the transition between two different topological phases.

Further increasing $\Delta H/(k_1\delta^2)$ moves the transitions towards and through critical points, where the transition is continuous, and into the crossover regime [Figs. 2(b) and 4(g)–4(i)]. The higher-temperature transitions become crossovers first as $\Delta H/(k_1\delta^2)$ increases until there is, eventually, a single crossover.

This results in significant melting of the SSI phases and the spontaneous production of defects. For each SSI phase there are two different types of defects. For a state obeying the spin-state ice rules everywhere changing a metal from a LS to HS state creates an h defect on both of the tetrahedra connected to the metal center [Figs. 5(a) and 5(b)]. Conversely, changing the spin state of a metal from HS to LS creates two ℓ defects.

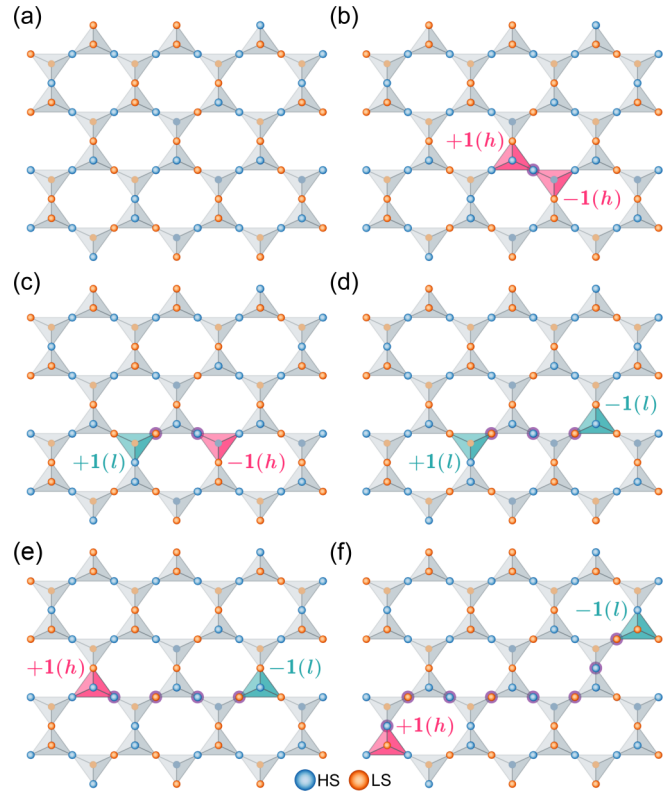

FIG. 5. Sketch of the propagation of defects in the H_2L_2 phase. (a) The H_2L_2 vacuum state: Every tetrahedron obeys the 2-HS/2-LS spin-state ice rule. (b) Changing the spin state of a LS metal center (highlighted in purple) creates h defects, on both tetrahedra connected to the metal, but does not change the total topological charge, $\sum Q = \sum \kappa \delta S$, where $\kappa = \pm 1$ for tetrahedra pointing in the $\pm z$ direction, and the sum runs over all tetrahedra. (c)–(f) Additional spin-state changes on tetrahedra hosting defects are a low-energy process that can cause the defects to propagate. This conserves Q, but not the numbers of h or ℓ defects. Similar processes result in deconfined excitations in both the H_1L_3 and H_3L_1 SSI phases.

To understand these defects it is helpful to consider a large magnetic field in the z direction, such that the component of the spin parallel to the field is $S_i^z(1) = S_H$ for HS metals and $S_i^z(-1) = S_L$ for LS metals. The creation of two h defects increases the number of HS metals by one. Thus, each defect carries a spin $\frac{1}{2}(S_H - S_L) \equiv \delta S$. Similarly, the process of creating two ℓ defects on the connected tetrahedra corresponds to the creation of two quasiparticles with spin $-\delta S$. It is important to note that there are no intermediate spin states in the model. Hence, these defects arise purely as a collective effect and thus correspond to fractionalized quasiparticles with spin midway between the HS and LS states.

The multiple ways to satisfy the spin-state ice rules allow defects to propagate (Fig. 5). For example, a metal center changing from HS to LS on a tetrahedron containing an h defect restores the ice rules on that tetrahedron and creates an ℓ defect on the other tetrahedron connected to the metal center [Figs. 5(b) and 5(c)]. Thus, the number of h- and

ℓ-type defects are not conserved. However, the topological charge $Q = \kappa\delta S$ is conserved, where $\kappa = \pm 1$ for tetrahedra pointing in the $\pm z$ direction. It only takes a finite amount of energy to move a pair of defects infinitely far apart. Hence, the fractionalized topological charges are deconfined [11].

h and ℓ defects carry the opposite spin. Therefore, if δS and $-\delta S$ topological charges meet on the same tetrahedron they annihilate, restoring the spin-state ice rules. This is analogous to electron-hole recombination in a semiconductor or matter-antimatter annihilation.

Passing a current through a molecule [53,54] or mechanically stretching or squeezing its ligands [21,55] can reversibly change its spin state; a voltage can switch between the two broken symmetry states of an antiferroelastically ordered chain [56]; and strain can induce the motion of domain walls in ordered phases of SCO materials [57]. These experiments suggest that applying a voltage or strain could also induce the motion of the defects in SSI phases, somewhat analogous to the current-induced motion of skyrmions [58,59]. Either of these effects could make SSI a valuable resource for spintronic applications.

IV. CONCLUSION

Our calculations predict that three distinct Coulomb phases arise in spin-crossover materials on pyrochlore lattices. In each phase the low-energy excitations are mobile and deconfined, carrying a spin midway between that of the HS and LS states. Realizing Coulomb phases beyond the two-in/two-out phases in water and spin ices has proven extremely challenging. However, the unique role of the single-molecule entropy in spin-crossover materials allows temperature and pressure to change the ice rules. The physics of SCO molecules could also allow for the use of pressure and light to manipulate and control the excitations.

Important questions arising from this work include the following: (1) What are the leading quantum mechanical corrections to the Hamiltonian? Exchange is weak but spin-orbit coupling is vital for the transition of a metal from HS to LS [60] and may act as a transverse field [61]. (2) What state do quantum mechanical corrections lead to? Is a single classical state selected (order by disorder) or does a "quantum spin-state liquid" emerge? Interestingly, an Ising model in the 3-HS/1-LS or 1-HS/3-LS states with an added transverse field term is closely related to the quantum dimer model on the diamond lattice, which is believed to host a gapless U(1) spin (state) liquid [62].

ACKNOWLEDGMENT

This work was funded by the Australian Research Council through Grant No. DP200100305 and an Australian Government Research Training Program Scholarship.

[1] C. Castelnovo, R. Moessner, and S. L. Sondhi, Spin ice, fractionalization and topological order, Annu. Rev. Condens. Matter Phys. **3**, 35 (2012).
[2] S. T. Bramwell and M. J. P. Gingras, Spin ice state in frustrated magnetic pyrochlore materials, Science **294**, 1495 (2001).
[3] M. J. Harris, S. T. Bramwell, D. F. McMorrow, T. Zeiske, and K. W. Godfrey, Geometrical Frustration in the Ferromagnetic Pyrochlore $Ho_2Ti_2O_7$, Phys. Rev. Lett. **79**, 2554 (1997).
[4] A. P. Ramirez, A. Hayashi, R. J. Cava, R. Siddharthan, and B. S. Shastry, Zero-point entropy in 'spin ice', Nature (London) **399**, 333 (1999).
[5] B. C. den Hertog and M. J. P. Gingras, Dipolar Interactions and Origin of Spin Ice in Ising Pyrochlore Magnets, Phys. Rev. Lett. **84**, 3430 (2000).
[6] S. T. Bramwell, M. J. Harris, B. C. den Hertog, M. J. P. Gingras, J. S. Gardner, D. F. McMorrow, A. R. Wildes, A. Cornelius, J. D. M. Champion, R. G. Melko, and T. Fennell, Spin Correlations in $Ho_2Ti_2O_7$: A Dipolar Spin Ice System, Phys. Rev. Lett. **87**, 047205 (2001).
[7] L. Pauling, The structure and entropy of ice and of other crystals with some randomness of atomic arrangement, J. Am. Chem. Soc. **57**, 2680 (1935).
[8] C. Castelnovo, R. Moessner, and S. L. Sondhi, Magnetic monopoles in spin ice, Nature (London) **451**, 42 (2008).
[9] D. J. P. Morris, D. A. Tennant, S. A. Grigera, B. Klemke, C. Castelnovo, R. Moessner, C. Czternasty, M. Meissner, K. C. Rule, J.-U. Hoffmann, K. Kiefer, S. Gerischer, D. Slobinsky, and R. S. Perry, Dirac strings and magnetic monopoles in spin ice $Dy_2Ti_2O_7$, Science **326**, 411 (2009).
[10] T. Fennell, P. P. Deen, A. R. Wildes, K. Schmalzl, D. Prabhakaran, A. T. Boothroyd, R. J. Aldus, D. F. McMorrow, and S. T. Bramwell, Magnetic Coulomb phase in the spin ice $Ho_2Ti_2O_7$, Science **326**, 415 (2009).
[11] C. L. Henley, Coulomb phases, Annu. Rev. Condens. Matter Phys. **1**, 179 (2010).
[12] M. J. P. Gingras and P. A. McClarty, Quantum spin ice: A search for gapless quantum spin liquids in pyrochlore magnets, Rep. Prog. Phys. **77**, 056501 (2014).
[13] L. Savary and L. Balents, Quantum spin liquids: A review, Rep. Prog. Phys. **80**, 16502 (2017).
[14] B. J. Powell, Emergent particles and gauge fields in quantum matter, Contemp. Phys. **61**, 96 (2020).
[15] T. Fennell, M. J. Harris, S. Calder, M. Ruminy, M. Boehm, P. Steffens, M.-H. Lemée-Cailleau, O. Zaharko, A. Cervellino, and S. T. Bramwell, Multiple Coulomb phase in the fluoride pyrochlore $CsNiCrF_6$, Nat. Phys. **15**, 60 (2019).
[16] P. W. Anderson, Ordering and Antiferromagnetism in Ferrites, Phys. Rev. **102**, 1008 (1956).
[17] E. Lefrançois, V. Cathelin, E. Lhotel, J. Robert, P. Lejay, C. V. Colin, B. Canals, F. Damay, J. Ollivier, B. Fåk, L. C. Chapon, R. Ballou, and V. Simonet, Fragmentation in spin ice from magnetic charge injection, Nat. Commun. **8**, 209 (2017).
[18] J. Cruddas and B. J. Powell, Spin-state ice in elastically frustrated spin-crossover materials, J. Am. Chem. Soc. **141**, 19790 (2019).
[19] P. Gütlich, Y. Garcia, and H. A. Goodwin, Spin crossover phenomena in Fe(II) complexes, Chem. Soc. Rev. **29**, 419 (2000).

[20] O. Kahn, J. Kröber, and C. Jay, Towards spin crossover applications, Adv. Mater. **4**, 718 (2004).

[21] A. Köbke, F. Gutzeit, F. Röhricht, A. Schlimm, J. Grunwald, F. Tuczek, M. Studniarek, D. Longo, F. Choueikani, E. Otero, P. Ohresser, S. Rohlf, S. Johannsen, F. Diekmann, K. Rossnagel, A. Weismann, T. Jasper-Toennies, C. Näther, R. Herges, R. Berndt, and M. Gruber, Reversible coordination-induced spin-state switching in complexes on metal surfaces, Nat. Nanotechnol. **15**, 18 (2020).

[22] H.-Z. Ye, C. Sun, and H. Jiang, Monte-Carlo simulations of spin-crossover phenomena based on a vibronic Ising-like model with realistic parameters, Phys. Chem. Chem. Phys. **17**, 6801 (2015).

[23] M. Paez-Espejo, M. Sy, and K. Boukheddaden, Elastic frustration causing two-step and multistep transitions in spin-crossover solids: Emergence of complex antiferroelastic structures, J. Am. Chem. Soc. **138**, 3202 (2016).

[24] C. Mariette, E. Trzop, J.-Y. Mevellec, A. Boucekkine, A. Ghoufi, G. Maurin, E. Collet, M. C. Muñoz, J. A. Real, and B. Toudic, Symmetry breakings in a metal organic framework with a confined guest, Phys. Rev. B **101**, 134103 (2020).

[25] J. Pavlik and R. Boča, Established static models of spin crossover, Eur. J. Inorg. Chem. **2013**, 697 (2013).

[26] M. Nishino, K. Boukheddaden, Y. Konishi, and S. Miyashita, Simple Two-Dimensional Model for the Elastic Origin of Cooperativity among Spin States of Spin-Crossover Complexes, Phys. Rev. Lett. **98**, 247203 (2007).

[27] M. Nishino and S. Miyashita, Termination of the Berezinskii-Kosterlitz-Thouless phase with a new critical universality in spin-crossover systems, Phys. Rev. B **92**, 184404 (2015).

[28] M. Nishino, C. Enachescu, and S. Miyashita, Multistep spin-crossover transitions induced by the interplay between short- and long-range interactions with frustration on a triangular lattice, Phys. Rev. B **100**, 134414 (2019).

[29] S. Miyashita, Y. Konishi, M. Nishino, H. Tokoro, and P. A. Rikvold, Realization of the mean-field universality class in spin-crossover materials, Phys. Rev. B **77**, 014105 (2008).

[30] T. Nakada, T. Mori, S. Miyashita, M. Nishino, S. Todo, W. Nicolazzi, and P. A. Rikvold, Critical temperature and correlation length of an elastic interaction model for spin-crossover materials, Phys. Rev. B **85**, 054408 (2012).

[31] M. Nishino and S. Miyashita, Effect of the short-range interaction on critical phenomena in elastic interaction systems, Phys. Rev. B **88**, 014108 (2013).

[32] H. Watanabe, K. Tanaka, N. Bréfuel, H. Cailleau, J.-F. Létard, S. Ravy, P. Fertey, M. Nishino, S. Miyashita, and E. Collet, Ordering phenomena of high-spin/low-spin states in stepwise spin-crossover materials described by the ANNNI model, Phys. Rev. B **93**, 014419 (2016).

[33] C. Enachescu, L. Stoleriu, M. Nishino, S. Miyashita, A. Stancu, M. Lorenc, R. Bertoni, H. Cailleau, and E. Collet, Theoretical approach for elastically driven cooperative switching of spin-crossover compounds impacted by an ultrashort laser pulse, Phys. Rev. B **95**, 224107 (2017).

[34] Y. Konishi, H. Tokoro, M. Nishino, and S. Miyashita, Monte Carlo Simulation of Pressure-Induced Phase Transitions in Spin-Crossover Materials, Phys. Rev. Lett. **100**, 067206 (2008).

[35] L. Stoleriu, P. Chakraborty, A. Hauser, A. Stancu, and C. Enachescu, Thermal hysteresis in spin-crossover compounds studied within the mechanoelastic model and its potential application to nanoparticles, Phys. Rev. B **84**, 134102 (2011).

[36] J. Cruddas and B. J. Powell, Structure-property relationships and the mechanisms of multistep transitions in spin crossover materials and frameworks, Inorg. Chem. Front. **7**, 4424 (2020).

[37] E. Collet, H. Watanabe, N. Bréfuel, L. Palatinus, L. Roudaut, L. Toupet, K. Tanaka, J.-P. Tuchagues, P. Fertey, S. Ravy, B. Toudic, and H. Cailleau, Aperiodic Spin State Ordering of Bistable Molecules and Its Photoinduced Erasing, Phys. Rev. Lett. **109**, 257206 (2012).

[38] J. E. Clements, J. R. Price, S. M. Neville, and C. J. Kepert, Hysteretic four-step spin crossover within a three-dimensional porous Hofmann-like material, Angew. Chem., Int. Ed. **55**, 15105 (2016).

[39] M. J. Murphy, K. A. Zenere, F. Ragon, P. D. Southon, C. J. Kepert, and S. M. Neville, Guest programmable multistep spin crossover in a porous 2-D Hofmann-type material, J. Am. Chem. Soc. **139**, 1330 (2017).

[40] M. Griffin, S. Shakespeare, H. J. Shepherd, C. J. Harding, J.-F. Létard, C. Desplanches, A. E. Goeta, J. A. K. Howard, A. K. Powell, V. Mereacre, Y. Garcia, A. D. Naik, H. Müller-Bunz, and G. G. Morgan, A symmetry-breaking spin-state transition in iron(III), Angew. Chem. Int. Ed. **50**, 896 (2011).

[41] Y. Sekine, M. Nihei, and H. Oshio, Dimensionally controlled assembly of an external stimuli-responsive $[Co_2Fe_2]$ complex into supramolecular hydrogen-bonded networks, Chem. Eur. J. **23**, 5193 (2017).

[42] N. Ortega-Villar, A. L. Thompson, M. C. Muñoz, V. M. Ugalde-Saldívar, A. E. Goeta, R. Moreno-Esparza, and J. A. Real, Solid- and solution-state studies of the novel μ-dicyanamide-bridged dinuclear spin-crossover system $[Fe(bztpen)]_2[\mu\text{-}N(CN)_2](PF_6)_3 \cdot nH_2O$, Chem. Eur. J. **11**, 5721 (2005).

[43] G. S. Matouzenko, D. Luneau, G. Molnár, N. Ould-Moussa, S. Zein, S. A. Borshch, A. Bousseksou, and F. Averseng, A two-step spin transition and order-disorder phenomena in the mononuclear compound $[Fe(Hpy\text{-}DAPP)](BF_4)_2$, Eur. J. Inorg. Chem. **13**, 2671 (2006).

[44] G. Ruzzi, J. Cruddas, R. H. McKenzie, and B. J. Powell, Equivalence of elastic and Ising models for spin crossover materials, arXiv:2008.08738.

[45] J. Wajnflasz and R. Pick, Transitions "low spin"-"high spin" dans les complexes de Fe^{2+}, J. Phys. Colloq. **32**, C1-91 (1971).

[46] Note that this approximation does not affect the phase diagrams in Fig. 2, but would curve the paths corresponding to fixed ΔH in Fig. 2(b), leading to concomitant qualitative changes in Fig. 4.

[47] W. Nicolazzi and A. Bousseksou, Thermodynamical aspects of the spin crossover phenomenon, C. R. Chim. **21**, 1060 (2018).

[48] E. Collet and P. Guionneau, Structural analysis of spin-crossover materials: From molecules to materials, C. R. Chim. **21**, 1133 (2018).

[49] A. J. McConnell, Spin-state switching in Fe(II) helicates and cages, Supramol. Chem. **30**, 858 (2018).

[50] See Supplemental Material at http://link.aps.org/supplemental/10.1103/PhysRevB.104.024433 for additional details of the Monte Carlo calculations, plots of the heat capacity, snapshots of the ice states, and the calculations of the spinodal lines.

[51] E. Milin, V. Patinec, S. Triki, E.-E. Bendeif, S. Pillet, M. Marchivie, G. Chastanet, and K. Boukheddaden,

Elastic frustration triggering photoinduced hidden hysteresis and multistability in a two-dimensional photoswitchable Hofmann-like spin-crossover metal-organic framework, Inorg. Chem. **55**, 11652 (2016).

[52] T. Boonprab, S. J. Lee, S. G. Telfer, K. S. Murray, W. Phonsri, G. Chastanet, E. Collet, E. Trzop, G. N. L. Jameson, P. Harding, and D. J. Harding, The first observation of hidden hysteresis in an iron(III) spin-crossover complex, Angew. Chem., Int. Ed. **58**, 11811 (2019).

[53] T. G. Gopakumar, F. Matino, H. Naggert, A. Bannwarth, F. Tuczek, and R. Berndt, Electron-induced spin crossover of single molecules in a bilayer on gold, Angew. Chem. Int. Ed. **51**, 6262 (2012).

[54] T. Miyamachi, M. Gruber, V. Davesne, M. Bowen, S. Boukari, L. Joly, F. Scheurer, G. Rogez, T. K. Yamada, P. Ohresser, E. Beaurepaire, and W. Wulfhekel, Robust spin crossover and memristance across a single molecule, Nat. Commun. **3**, 938 (2012).

[55] G. Kuang, Q. Zhang, T. Lin, R. Pang, X. Shi, H. Xu, and N. Lin, Mechanically-controlled reversible spin crossover of single Fe-porphyrin molecules, ACS Nano **11**, 6295 (2017).

[56] J. Liu, Y. Gao, T. Wang, Q. Xue, M. Hua, Y. Wang, L. Huang, and N. Lin, Collective spin manipulation in antiferroelastic spin-crossover metallo-supramolecular chains, ACS Nano **14**, 11283 (2020).

[57] V. B. Jakobsen, E. Trzop, L. C. Gavin, E. Dobbelaar, S. Chikara, X. Ding, K. Esien, H. Müller-Bunz, S. Felton, V. S. Zapf, E. Collet, M. A. Carpenter, and G. G. Morgan, Stress-induced domain wall motion in a ferroelastic Mn^{3+} spin crossover complex, Angew. Chem., Int. Ed. **59**, 13305 (2020).

[58] A. Fert, N. Reyren, and V. Cros, Magnetic skyrmions: Advances in physics and potential applications, Nat. Rev. Mater. **2**, 17031 (2017).

[59] I. A. Ado, O. A. Tretiakov, and M. Titov, Microscopic theory of spin-orbit torques in two dimensions, Phys. Rev. B **95**, 094401 (2017).

[60] E. Buhks, G. Navon, M. Bixon, and J. Jortner, Spin conversion processes in solutions, J. Am. Chem. Soc. **102**, 2918 (1980).

[61] G. D'Avino, A. Painelli, and K. Boukheddaden, Vibronic model for spin crossover complexes, Phys. Rev. B **84**, 104119 (2011).

[62] R. Moessner and K. S. Raman, *Quantum dimer models, in Introduction to Frustrated Magnetism: Materials, Experiments, Theory*, edited by C. Lacroix, P. Mendels, and F. Mila (Springer, Berlin, 2011), Chap. 17, pp. 437–479.